Acta Crystallographica Section D
Biological Crystallography
ISSN 1399-0047

Structural insights into the catalytic mechanism of human squalene synthase

Chia-I Liu,[a,b,c] Wen-Yih Jeng,[d] Wei-Jung Chang,[a,b] Min-Fang Shih,[a,b] Tzu-Ping Ko[a,b] and Andrew H.-J. Wang[a,b,e]*

[a]Institute of Biological Chemistry, Academia Sinica, Taipei 11529, Taiwan, [b]Core Facilities for Protein Structural Analysis, Academia Sinica, Taipei 11529, Taiwan, [c]School of Medical Laboratory Science and Biotechnology, College of Medical Science and Technology, Taipei Medical University, Taipei 10031, Taiwan, [d]University Center for Bioscience and Biotechnology, National Cheng Kung University, Tainan 70101, Taiwan, and [e]College of Medical Science and Technology, Taipei Medical University, Taipei 10031, Taiwan

Correspondence e-mail: ahjwang@gate.sinica.edu.tw

Received 29 July 2013
Accepted 23 September 2013

PDB References: *h*SQS–FsPP, 3wef; *h*SQS–FsPP–Mg^{2+}, 3weg; *h*SQS–PSPP–Mg^{2+}, 3weh; *h*SQS-(Y73A)–PSPP–Mn^{2+}, 3wei; *h*SQS-(F288A)–PSPP–Mg^{2+}, 3wej; *h*SQS-(F288L)–PSPP–Mg^{2+}, 3wek

Squalene synthase (SQS) is a divalent metal-ion-dependent enzyme that catalyzes the two-step reductive 'head-to-head' condensation of two molecules of farnesyl pyrophosphate to form squalene using presqualene diphosphate (PSPP) as an intermediate. In this paper, the structures of human SQS and its mutants in complex with several substrate analogues and intermediates coordinated with Mg^{2+} or Mn^{2+} are presented, which stepwise delineate the biosynthetic pathway. Extensive study of the SQS active site has identified several critical residues that are involved in binding reduced nicotinamide dinucleotide phosphate (NADPH). Based on mutagenesis data and a locally closed (JK loop-in) structure observed in the *h*SQS-(F288L)–PSPP complex, an NADPH-binding model is proposed for SQS. The results identified four major steps (substrate binding, condensation, intermediate formation and translocation) of the ordered sequential mechanisms involved in the '1′–1' isoprenoid biosynthetic pathway. These new findings clarify previous hypotheses based on site-directed mutagenesis and biochemical analysis.

1. Introduction

Cyclic triterpenoids derived from squalene (SQ) are widely distributed in eukaryotes (sterols) and prokaryotes (hopanoids). Their contributions are critical determinants of membrane fluidity and permeability, and sterols also serve as hormone precursors and secondary messengers in developmental signalling. The final triterpenoid products are cholesterol in mammals, ergosterols in fungi and protozoa, and phytosterols in plants. On the other hand, a wide range of bacteria produce hopene and related hopanoids as sterol surrogates. The down-regulation of specific sterol biosynthesis serves as a potential selective target to control diseases associated with hypercholesterolaemia and infections caused by fungi and parasites.

Squalene synthase (SQS) has been cloned from a broad range of eukaryotes as well as the bacterial strains *Thermosynechococcus elongatus*, *Bradyrhizobium japonicum* and *Zymomonas mobilis* (Perzl *et al.*, 1998; Lee & Poulter, 2008). The eukaryotic SQS is anchored to the membrane by a short C-terminal transmembrane helix which is absent in the bacterial enzymes. Human SQS (*h*SQS) catalyzes the first step of cholesterol biosynthesis, in which two farnesyl pyrophosphate (FPP) molecules are condensed in a 'head-to-head' or '1′–1' coupling to form SQ. The catalytic process involves two reactions: firstly, two FPP molecules are condensed to form presqualene diphosphate (PSPP), an intermediate with a cyclopropane C1′–C2–C3 ring structure; secondly, PSPP

undergoes a nicotinamide adenine dinucleotide phosphate (NADPH)-dependent rearrangement and reduction to generate the end product SQ, as outlined in Fig. 1. The reaction follows the ordered mechanism proposed for yeast SQS (*y*SQS) using steady-state kinetic measurements, in which two FPP molecules bind to the enzyme before NADPH (Mookhtiar *et al.*, 1994). Furthermore, the presence of NADPH specifically stimulates the formation of PSPP (Radisky & Poulter, 2000). If NADPH is absent PSPP is solvolyzed slowly, yielding a mixture of six triterpene hydrocarbons and alcohols with 1′–1 or 1′–3 skeletons (Jarstfer *et al.*, 2002). In addition, the formation of PSPP or substrate-induced conformational changes in *y*SQS has been proposed to be the rate-limiting step in the reaction (Mookhtiar *et al.*, 1994).

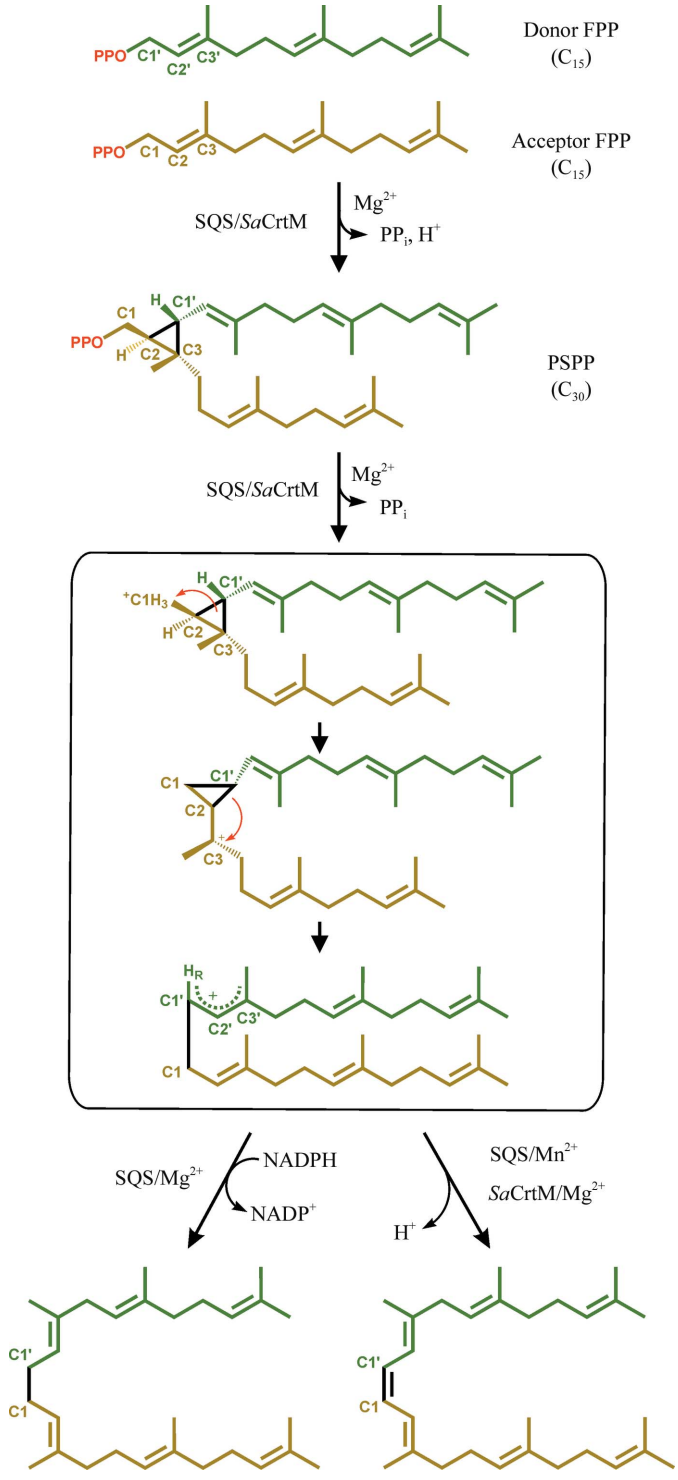

Figure 1
Chemical reactions catalyzed by squalene synthase (SQS). In the presence of Mg^{2+} and NADPH, FPP is efficiently converted into squalene. In the absence of NADPH and in the presence of Mn^{2+}, PSPP is converted to dehydrosqualene as the major product (identical to the final product of *Sa*CrtM in the presence of Mg^{2+}). The 1′–2 and 1′–3 linkages of the C1′–C2–C3 tripterpene PSPP are broken, forming 1′–1 fused products. FPP, farnesyl pyrophosphate; PSPP, presqualene diphosphate.

Only a few enzymes have been found to catalyze 'head-to-head' condensation. Similar reactions that form the C_{30} PSPP and the C_{40} PPPP (prephytoene diphosphate) occur in *Staphylococcus aureus* dehydrosqualene synthase (*Sa*CrtM; Pelz *et al.*, 2005; Lin *et al.*, 2010) and in phytoene synthase (PSY) from photosynthetic organisms (Dogbo *et al.*, 1988; Iwata-Reuyl *et al.*, 2003), respectively. The cyclopropane ring-containing PSPP and PPPP are precursors for the biosynthesis of bacterial pigments and carotenoids. Unlike SQS, both enzymes eliminate a proton and do not utilize NADPH. One double bond not found in squalene is retained between the C1 and C1′ atoms of the C_{30} and C_{40} hydrocarbon species. In the presence of Mn^{2+} and in the absence of NADPH, PSPP was converted to dehydrosqualene (an *Sa*CrtM product) as the main product in yeast (Jarstfer *et al.*, 2002) and *Arabidopsis thaliana* SQS (Nakashima *et al.*, 1995). Because SQS and *Sa*CrtM share sequence homology and have similar protein scaffolds for enzymatic catalysis; the superposed active site can act as a target for a dual-inhibitor design for cholesterol-lowering and anti-infective agents (Kahlon *et al.*, 2010; Lin *et al.*, 2012; Liu *et al.*, 2012). However, the sequences of *h*SQS and PSY exhibit only a low level of homology. Previously, we reported a structure-based mechanism of *Sa*CrtM (Lin *et al.*, 2010) and the targeting of the fungal metabolite zaragozic acid A (ZA-A) to *Sa*CrtM and *h*SQS as a potential inhibitor (Liu *et al.*, 2012). Although the structures of apo and inhibitor-bound *h*SQS have been solved (Liu *et al.*, 2012), the active-site configuration does not provide substantial information concerning the catalytic process.

In this paper, we report a series of structures of *h*SQS in complex with substrates and intermediates that represent major steps along the reaction path from substrate binding and condensation to intermediate formation and translocation into the active site. This process is exquisitely regulated by divalent metal ions. We conclude that these principal mechanistic features of the catalytic process are common to other 'head-to-head' terpene synthases. Furthermore, we explicitly explain the structure-based catalytic role of Phe288 for the first time. We analyzed the role of key conserved residues in the reaction mechanism. Finally, by combining the site-directed mutagenesis data and a locally closed (JK loop-in) structure observed in the F288L–PSPP complex, we propose a plausible NADPH-binding model in SQS. The information from these sources clarifies previous hypotheses based on site-directed mutagenesis and biochemical analyses.

Table 1
Data-collection and refinement statistics.

Values in parentheses are for the outermost resolution shell.

	*h*SQS–FsPP (without Mg^{2+})	*h*SQS–FsPP–Mg^{2+}	*h*SQS–PSPP–Mg^{2+}	*h*SQS-(F288A)–PSPP–Mg^{2+}	*h*SQS-(F288L)–PSPP–Mg^{2+}	*h*SQS-(Y73A)–PSPP–Mn^{2+}
Crystal form	Form III	Form II	Form I	Form I	Form II	Form II
PDB code	3wef	3weg	3weh	3wej	3wek	3wei
Molecules per asymmetric unit	6	1	1	1	1	1
Data collection						
Radiation source	Rigaku FR-E	17A, PF	NW12, PF	BL13B1, NSRRC	BL13B1, NSRRC	BL44XU, SPring-8
Wavelength (Å)	1.54178	0.98000	1.00000	1.00000	1.00000	0.90000
Space group	$P2_1$	$P2_12_12$	$P2_12_12_1$	$P2_12_12_1$	$P2_12_12$	$P2_12_12$
Unit-cell parameters						
a (Å)	85.89	94.37	36.24	35.71	94.19	94.19
b (Å)	153.75	106.72	93.88	94.50	106.50	106.31
c (Å)	91.61	33.57	108.80	105.31	32.99	33.11
β (°)	91.06					
Resolution (Å)	30–2.35 (2.43–2.35)	30–1.75 (1.81–1.75)	30–1.87 (1.94–1.87)	30–2.00 (2.07–2.00)	30–1.85 (1.92–1.85)	30–1.79 (1.85–1.79)
No. of reflections	97910 (9672)	34977 (3397)	31534 (3095)	24564 (2388)	29252 (2834)	32223 (3164)
Completeness (%)	99.1 (98.7)	99.3 (99.1)	99.8 (100)	99.4 (99.6)	99.8 (99.5)	99.9 (100)
Multiplicity	4.6 (4.3)	5.9 (4.6)	5.8 (5.9)	4.6 (4.4)	5.0 (4.6)	7.0 (7.1)
R_{merge} (%)	7.9 (65.5)	8.8 (52.3)	5.7 (51.7)	9.2 (52.0)	8.6 (49.9)	7.1 (50.3)
$\langle I/\sigma(I)\rangle$	23.0 (3.6)	27.5 (3.3)	30.5 (4.5)	18.5 (3.0)	16.7 (2.0)	30.4 (4.4)
Overall Wilson *B* factor ($Å^2$)	49.7	28.4	32.1	30.5	28.9	27.2
Refinement						
No. of reflections						
Work set	92805 (13094)	33037 (4682)	29759 (4175)	23121 (3218)	27594 (3926)	30450 (4357)
Free set	4876 (714)	1740 (267)	1583 (234)	1249 (188)	1473 (223)	1626 (234)
R_{work} (%)	19.0 (23.9)	15.5 (19.6)	16.4 (18.7)	20.8 (25.2)	22.5 (30.7)	15.0 (19.3)
R_{free} (%)	25.7 (32.9)	20.8 (27.8)	21.8 (27.1)	27.6 (31.0)	25.7 (33.0)	20.9 (28.0)
R.m.s.d., bond lengths (Å)	0.007	0.007	0.007	0.007	0.007	0.007
R.m.s.d., bond angles (°)	1.4	1.4	1.4	1.4	1.4	1.4
No. of atoms						
Protein	15961	2702	2681	2699	2702	2695
Compound	192	48	39	39	39	39
Ions		3	2	2	1	3
Water molecules	352	283	293	249	223	302
Mean *B* values ($Å^2$)						
Protein	54.6	23.6	26.3	26.7	27.9	24.2
Compound	81.8	64.3	29.3	42.4	38.4	40.2
Ions		47.2	17.9	29.6	39.7	32.6
Water molecules	48.0	36.5	43.0	34.4	36.7	37.6
Ramachandran plot, residues in (%)						
Favoured region	96.9	98.2	99.1	98.2	99.1	98.8
Allowed region	3.1	1.8	0.9	1.8	0.9	1.2

2. Materials and methods

2.1. Materials

Ni–NTA Sepharose resin was purchased from GE Healthcare Life Sciences, Uppsala, Sweden. Thrombin was purchased from Novagen, Madison, USA. Crystallization reagents were purchased from Hampton Research, California, USA. All other chemicals used in this research were purchased from Sigma–Aldrich, Missouri, USA and Fluka, Buchs, Switzerland.

2.2. Expression, purification and crystallization

Protein expression and crystallization of doubly truncated *h*SQS (31–370) were performed according to a previously described method (Liu *et al.*, 2012). In brief, the truncated gene was cloned into pET-28a with an N-terminal His tag followed by a thrombin protease recognition site. The constructs were transformed into *Escherichia coli* expression strain BL21 (DE3). The His-tagged recombinant protein was purified and the N-terminal His tag was then cleaved using thrombin and removed using Ni–NTA Sepharose. The protein concentration was determined using the Bradford method (Bio-Rad Protein Assay kit) with bovine serum albumin as the standard.

We obtained three types of crystal form in this study. Forms I and II contain a monomer in the asymmetric unit, while the protein in the form III crystals assembles into a hexamer with two trimers related by twofold symmetry. The crystals were grown by mixing equal volumes of protein solution and precipitant solution (form I, 20% PEG 2K MME, 0.01 *M* $NiCl_2$, 0.1 *M* Tris pH 8.5; form II, 1.4 *M* sodium citrate tribasic dehydrate, 0.1 *M* Na HEPES pH 7.5; form III, 2 *M* K_2HPO_4/NaH_2PO_4 pH 6.5) at 298 K. The cocrystallization solution contained the *h*SQS protein (at 10 mg ml^{-1}) with 3 m*M* FsPP in the absence and presence of 1 m*M* Mg^{2+} or with 1 m*M* PSPP and 1 m*M* Mg^{2+} in order to analyze how the enzyme recognizes the substrates and to elucidate its reaction mechanism. The crystals of the *h*SQS-(F288A)–PSPP–Mg^{2+}, *h*SQS-(F288L)–PSPP–Mg^{2+} and *h*SQS-(Y73A)–PSPP–Mn^{2+} complexes were obtained under similar conditions. 1 m*M* PSPP and 1 m*M* Mg^{2+} or 3 m*M* Mn^{2+} were cocrystallized with

*h*SQS mutants to obtain protein complexes. The hanging-drop vapour-diffusion method was employed in all crystallization experiments.

2.3. Data collection, structure determination and refinement

The diffraction data of the *h*SQS (31–370) complex crystals were collected using a Rigaku FR-E SuperBright generator at the Institute of Biological Chemistry, Academia Sinica and on beamlines 13B1 and 13C1 of the National Synchrotron Radiation Research Center (NSRRC) in Taiwan, on beamlines 17A and NW12 of the Photon Factory (PF) and on beamline BL44XU at SPring-8 in Japan. All diffraction data were processed and scaled using the *HKL*-2000 package (Otwinowski & Minor, 1997). The structures of the *h*SQS (31–370) complexes were solved by molecular replacement using *MOLREP* (Vagin & Teplyakov, 2010), in which the structure of apo *h*SQS (31–370) from our previous work served as a search model (PDB entries 3vjb and 3vj8; Liu *et al.*, 2012). Iterative model building and computational refinement were performed using *Coot* (Emsley & Cowtan, 2004) and *REFMAC*5 (Murshudov *et al.*, 2011). Manual rebuilding of the models used both $2F_o - F_c$ and $F_o - F_c$ electron-density maps. *RAMPAGE* (Lovell *et al.*, 2003) was used to calculate Ramachandran plots, to identify and correct rotamer outliers and to identify potential steric clashes in the models. Figures illustrating the crystal structures and superpositions were prepared using *PyMOL* (Schrödinger; http://www.pymol.org/). Data-collection and refinement statistics can be found in Table 1.

2.4. Site-directed mutagenesis of human squalene synthase

The SQS mutants were prepared using the QuikChange site-directed mutagenesis kit (Stratagene) in conjunction with the human SQS gene template in the pET-28a vector. The mutagenic oligonucleotides for performing site-directed mutagenesis are listed in Supplementary Table S1[1]. The mutation was confirmed by DNA sequencing. Each purified mutant SQS was verified by mass-spectrometric analysis and its purity (>95%) was checked using SDS–PAGE.

2.5. Measurement of squalene synthase activity

The activity of *h*SQS was determined by measuring FPP consumption, PSPP accumulation and squalene formation using HPLC. The quantification of these products was performed in triplicate, as described by Jarstfer and coworkers with slight modifications (Gu *et al.*, 1998; Jarstfer *et al.*, 2002), on an UltiMate 3000 UHPLC$^+$ Focused system (Thermo Fisher Scientific, Waltham, Massachusetts, USA) equipped with an UltiMate 3000 Pump, an UltiMate 3000 autosampler and a diode-array detector (Dionex Diode Array Detector DAD-3000RS, Dionex) recording at 214 nm. Typically, each reaction contained 0.05 µmol FPP (Sigma), 0.1 µmol NADPH (Sigma) and 20 µg recombinant *h*SQS in reaction buffer (35 m*M* MOPS pH 7.2, 5 m*M* $MgCl_2$, 0.5 m*M* DTT, 0.3 mg ml^{-1} BSA) with a total volume of 105 µl. Because of the high specificity of the separation and detection system, small volumes of the reaction sample (100 µl) were injected directly without prior sample extraction. The amounts of FPP and PSPP were measured using reverse-phase HPLC on a C18 column (YMC S-5; 250 × 4.6 mm, 5 µm) with a linear solvent gradient of 0–100% acetonitrile in 25 m*M* ammonium hydrogen carbonate pH 8.0 in 35 min. Squalene was detected using normal-phase HPLC on a Hypersil silica column (Thermo; 250 × 4.6 mm, 5 µm) in 95% hexane with 5% methyl *t*-butyl ether as the mobile phase. The column temperature was maintained at 303 K. The liquid-chromatography flow rate was 1 ml min^{-1}. All terpene synthases require divalent metal ions, usually Mg^{2+}, for the catalytic process. To investigate the effect of different divalent ions, the same experiments were performed in the presence of varying concentrations of $MgCl_2$ or $MnCl_2$ (0–10 m*M*). To determine the HPLC retention times of FPP, PSPP and squalene, the reaction molecules from *h*SQS were collected, the solvent was removed under a vacuum and the molecules were analyzed using ESI (FPP and PSPP) or EI (squalene) mass spectrometry to determine the molecular weight. Squalene was observed at an MS (EI) *m*/*z* value of 410.39 $(M + H)^+$; FPP and PSPP were observed at MS (ESI) *m*/*z* values of 381.12 and 585.31 $(M + H)^+$.

2.6. Structural modelling

The protein structure from *h*SQS-(F288L)–PSPP–Mg^{2+} (JK loop-in conformation) was modelled in complex with PSPP–Mg^{2+} [from *h*SQS-(Y73A)–PSPP–Mn^{2+}; PDB entry 3wei] and NADPH (modelled) to represent the *h*SQS–PSPP–Mg^{2+}–NADPH complex. The structure was validated using various programs. The modelled structure of NADPH was generated by *Coot* (Emsley & Cowtan, 2004) and optimized by energy minimization using *REFMAC*5 (Murshudov *et al.*, 2011) in the *CCP*4 suite (Winn *et al.*, 2011). The structural figures were produced using *PyMOL*.

3. Results and discussion

3.1. Overall structure

Structures of truncated *h*SQS bound to either substrate analogue with and without Mg^{2+} or to intermediates in the presence of Mg^{2+} and of its mutants in complex with intermediates and Mg^{2+} or Mn^{2+} were obtained. Three crystal forms of *h*SQS were used in structure determination: one monoclinic ($P2_1$, six molecules per asymmetric unit) and two orthorhombic ($P2_12_12_1$ and $P2_12_12$, one molecule per asymmetric unit). The stereochemical factors of the final models were analyzed by *RAMPAGE* (Lovell *et al.*, 2003) and *SFCHECK* (Vaguine *et al.*, 1999) from the *CCP*4 suite. The doubly truncated *h*SQS structure is primarily an α-helical bundle fold (Fig. 2*a*) and differs from other typical NADPH-dependent enzymes, which contain the highly conserved Rossmann-fold core for catalysis. A centrally located cavity surrounded by the conserved regions I–IV constitutes the

[1] Supporting information has been deposited in the IUCr electronic archive (Reference: MH5106).

hydrophobic core of the protein active site (Supplementary Fig. S1*b*). The conserved Asp-rich motifs found in helices αC (^{80}D*XX*ED^{84}) and αH (^{219}D*XX*ED^{223}) face the central cavity, with the carboxylic groups approximately 11 Å apart (Supplementary Fig. S1*a*). In agreement with other *trans*-prenyltransferases, the highly conserved Asp residues in the two Asp-rich motifs are coordinated to the catalytic Mg^{2+} ion involved in allylic substrate recognition. The introduction of mutations in this region eliminated or abolished the enzyme activity in various SQSs and the homologous *Sa*CrtM (Gu *et al.*, 1998; Lin *et al.*, 2010; Zhao *et al.*, 2010). In *h*SQS, one side of the central cavity is buttressed by two mobile segments, the AB flap (^{51}SRSF^{54}) and the JK loop (^{314}VKIRK^{318}) and helix αK, which are assumed to regulate the binding of substrates (prenyl donor and acceptor) and NADPH (Figs. 2*a* and 1*b*; Pandit *et al.*, 2000). Helix αK in the monoclinic $P2_1$ structure (the *h*SQS–FsPP complex) presents a flap-out conformation, but the electron-density map of this region in chains *A*, *D*, *E* and *F* is not clearly visible. We assume that this flexibility is responsible for recruitment of NADPH into the active site. To address how the ligands are bound in the ordered sequential mechanism and how the critical residues are involved in the catalytic process, the substrate and the intermediate complexes at various stages are presented (Figs. 2*c*–2*h*).

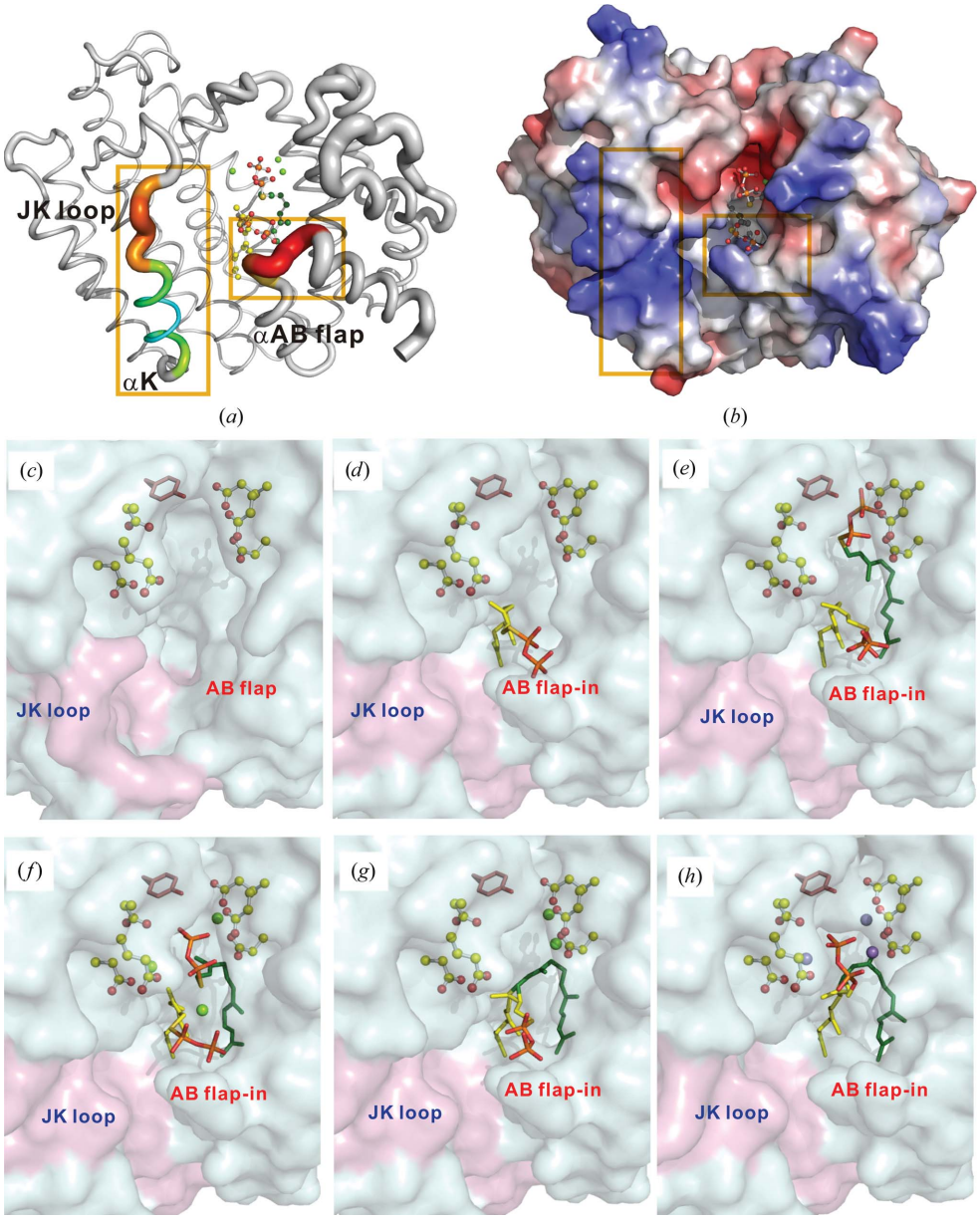

Figure 2
(*a*) Overall structure of the *h*SQS–FsPP–Mg^{2+} complex. The two molecules of FsPP, S1 FsPP (green) and S2 FsPP (yellow), bound to the active site are shown as ball-and-stick models. The two golden boxes highlight the flexible regions in ligand binding. The coloured ribbon model is based on *B* factors, with red representing a high *B* factor and deep blue representing a lower *B* factor. (*b*) Electrostatic surface-potential representation of the *h*SQS–FsPP–Mg^{2+} complex structure. The two flexible regions are mostly composed of multiply positively charged residues surrounding the active site. (*c*)–(*h*) Structures at various steps of the the *h*SQS reaction. The *h*SQS active site is shown as a molecular surface in cyan; the pink colour highlights the unique and highly conserved region IV of SQS. The two aspartate-rich motifs are shown in ball-and-stick representation and Tyr171 is shown as a stick model. (*c*) Apo structure (PDB entry 3vj8). (*d*) The enzyme with a bound S2 FsPP (acceptor; yellow). (*e*) Ternary complex with S1 FsPP (donor; green) and S2 FsPP. (*f*) Ternary complex with S1 FsPP, S2 FsPP and a trio of Mg^{2+} ions. (*g*) Binary complex with PSPP and two Mg^{2+} ions. (*h*) Binary complex with PSPP and a trio of Mn^{2+} ions. The Mg^{2+} and Mn^{2+} ions are shown as green and purple balls, respectively.

3.2. Catalytic mechanism

3.2.1. Step 1: substrate binding. SQS is a monomeric enzyme that performs two consecutive reactions. The identical first half-reaction of the catalytic mechanism and the similarity in the protein architectures of *h*SQS and *Sa*CrtM imply that SQS adopts the S1 site as the 'activating binding site' (the ionization site) to bind the prenyl donor and the S2 site as the 'non-activating binding site' for occupancy by the prenyl acceptor (alkene-donor site) (Lin *et al.*, 2010).

To determine the structural features that govern the substrate binding and catalysis of *h*SQS, we crystallized a trapped enzyme–substrate complex. The crystal of *h*SQS–FsPP was first grown in a divalent ion-free condition bound to one or two molecules of the noncleavable FPP analogue FsPP

(farnesyl thiopyrophosphate). The structure belonged to space group $P2_1$, and is unique with regard to the formation of a hexameric assembly with two trimers (denoted *A*–*F*) per asymmetric unit (Supplementary Fig. S2). Chains *C* and *D* are each bound to one FsPP molecule (S2 FsPP), while chains *A*, *B* and *E* bind two molecules (S1 FsPP and S2 FsPP); chain *F* is ligand-free. Several specific hydrogen bonds and many specific van der Waals contacts for ligand recognition were observed in the active site. In contrast to the S1 FsPP binding region, the S2 site presents a straighter tunnel to the centre (Fig. 2*d*). Mookhtiar *et al.* (1994) also found the presence of two different affinity binding sites in *y*SQS based on a kinetic assay (Mookhtiar *et al.*, 1994). The S2 FsPP (shown in yellow) binds to the S2 site and its pyrophosphate group is bound through hydrogen bonds to residues Ser51 and Ser53 on the AB flap. As shown by the comparison of chains *A*–*E* in Supplementary Fig. S2, the head groups of both FsPP molecules adopt various orientations. We also observed weak electron density for the first isoprene unit of S1 FsPP (shown in green), indicating its flexibility. S1 FsPP, which might act as a prenyl donor, is bound adjacent to the D*XX*ED motifs and to the conserved Tyr171 (Figs. 2*e* and 3*a*). The crystal structure of the *h*SQS complex with one or two molecules of FsPP implies an ordered binding mechanism: the S2 FsPP binds first and is followed by the S1 FsPP. The binding of the S2 FPP stabilizes an AB flap-in conformation and slightly changes the position of Tyr73. The S1 FsPP allylic group is layered between the hydrophobic polyprenyl moieties of S2 FsPP and the wall of the hydrophobic cavity in the active site. Hydrophobic residues such as Tyr73, Leu76, Met150, Met154, Met175 and Val179, which form the inner cavity of the S1 binding site, contribute significantly to the stability of the position and the orientation of the FsPP aliphatic moiety. As revealed by the structures, the bottom of the S1 site is delimited by the hydrophobic side chains of Val69, Leu183 and Phe288. Another bulky residue, Tyr276 in helix αI, forms a second hydrophobic floor for the apolar tail of S2 FsPP.

3.2.2. Step 2: the condensation of two substrates to form an intermediate with a cyclopropane ring. During the condensation process, two FPP molecules must be close to each other for the alkyl donor to attack the alkene acceptor. The Mg^{2+} ions that play a crucial role in fixing and activating the diphosphate moeity to yield an allylic cation by releasing a pyrophosphate group inside the active site have been found in both *cis*- and *trans*-polyprenyl diphosphate synthases (Liang, 2009), as well as in terpene cyclases (Cao *et al.*, 2010). Certain residues, particularly the Asp in the 'Asp-rich' motif, might assist in the Mg^{2+} migration and thus initiate the condensation reaction through ionization of the pyrophosphate group from the alkyl donor. As mentioned previously, the FsPP bound to the S1 site is flexible, particularly in the pyrophosphate group and the first isoprene unit, which exhibit diverse binding patterns in the active site. SQS uses either Mg^{2+} or Mn^{2+} to stimulate activity and forms identical products in the presence of NADPH. In divalent ion-free buffers, no activity was observed. An optimal activity was obtained using 5 m*M* Mg^{2+} or 0.5 m*M* Mn^{2+} (Supplementary Fig. S3*a*). However, inhibition occurred at higher concentrations of Mn^{2+} (>2 m*M*). In the structure of *h*SQS–FsPP–Mg^{2+}, *h*SQS also binds to the pyrophosphate of S1 FsPP through a trio of Mg^{2+} ions coordinated by two D*XX*ED motifs and promotes further ionization (Figs. 2*f* and 3*b*). Asp80, Glu83 and Asp84 of the first Asp-rich motif in helix αC make coordinating interactions with $Mg1^{2+}$ and $Mg2^{2+}$. The first aspartate of the second Asp-rich motif, Asp219 in helix αH, coordinates to $Mg3^{2+}$. A similar trinuclear metal cluster for activation of a 'head-to-tail' alkylation

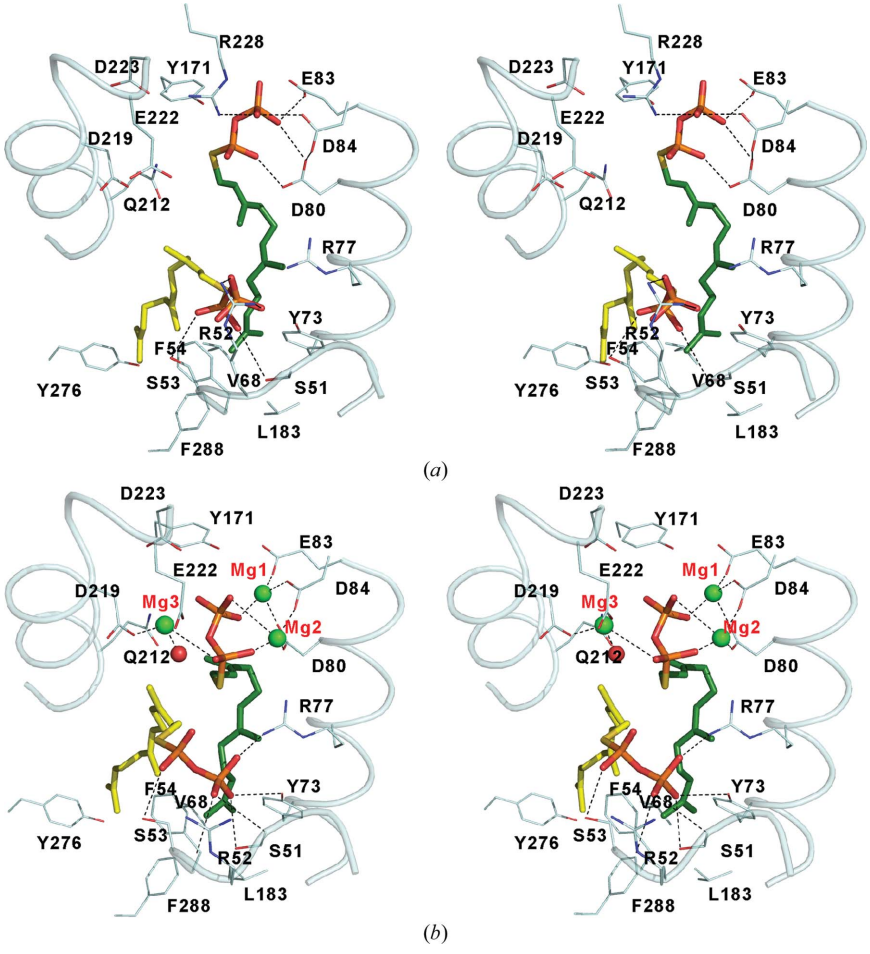

Figure 3
X-ray structures of *h*SQS with the substrate analogue FsPP and the intermediate PSPP in the absence and presence of Mg^{2+} or Mn^{2+}. The side chains of residues around the active site of *h*SQS are shown as thin stick models. The ligands are presented as thick sticks. Mg^{2+} and Mn^{2+} ions are presented as green and purple balls, respectively. (*a*) Stereoview of FsPP bound to *h*SQS in the absence of Mg^{2+} (chain *E*; PDB entry 3wef).

reaction through two Asp-rich motifs has also been found in many *trans*-prenyltransferases. The sequential ionization condensation–elimination mechanism has been adapted in *trans*-prenyltransferases, starting with a triple Mg^{2+} cluster-triggered ionization step, such as that found in FPPS (farnesyl pyrophosphate synthase; Rondeau *et al.*, 2006), GGPPS (geranylgeranyl pyrophosphate synthase; Guo *et al.*, 2007), TEAS (tobacco 5-epi-epiaristolochene synthase; Starks *et al.*, 1997) and limonene synthase (Hyatt *et al.*, 2007).

Determining how the '1′–1' condensation reaction occurs requires consideration of how the Asp residues and Mg^{2+} assist in the migration of S1 FPP towards S2 FPP, thus probably initiating the condensation reaction by adding the farnesyl unit of S1 FPP to the C2═C3 double bond of S2 FPP. The cyclopropanation reaction and the reducing process have been studied by Poulter and coworkers (Radisky & Poulter, 2000; Jarstfer *et al.*, 2002; Blagg *et al.*, 2002). The reaction is initiated by cleaving the C—O diphosphate bond of S1 FPP, forming an allylic carbocation–pyrophosphate ion pair. This highly unstable intermediate can then be nucleophilically attacked by the 2,3-π bond of S2 FPP, with concomitant proton loss, to form PSPP. As shown in Figs. 2(*f*) and 3(*b*), the distance between the C1′ atom of S1 FsPP and the C2═C3 double bond of S2 FsPP presented in this study was approximately 4 Å and it may become even shorter during catalysis. The initial carbocation intermediate (or the carbocation from the allylic substrate) may be stabilized by electrostatic interactions with a magnesium-bound pyrophosphate moiety and also through the side chain of Gln212. The substitution of Gln212 by Glu did not influence squalene formation. Whereas both the Q212L and the Q212N mutants completely aborted squalene production, the Q212N mutant retained approximately 50% of the first-step activity (Supplementary Table S2). The side chains of Arg77 and Arg228, which are oriented toward the central cleft and near the two pyrophosphate heads of the substrate, might serve as a pyrophosphate carrier for subsequent pyrophosphate release. We found that alteration of Arg228 did not significantly affect the substrate consumption; rather, a change of Arg77 to Ala led to an obvious decrease in enzyme activity, indicating its critical role in catalysis.

Rilling (1966) discovered that accumulation of PSPP occurred if NADPH was removed from the reaction buffer. The cyclopropyl-containing intermediate is temporarily stable and can be purified (Supplementary Fig. S3*c*). The structure of the *h*SQS–PSPP–Mg^{2+} complex (PDB entry 3weh) shows that the structural features governing PSPP binding are similar to the previously determined structure of *Sa*CrtM (PDB entry 3adz; Lin *et al.*, 2010), with a root-mean-square deviation (r.m.s.d.) of 2.5 Å between 253 C^{α} atoms, although the relative orientations of the pyrophosphate group are different. The pyrophosphate head lies near the AB flap (the non-activating site) and the two hydrophobic allylic tails remain bound to the S1 site along with the S2 site (Figs. 2*g* and 3*c*). The first isoprene unit of S1 FsPP, which bends to link to S2 FsPP, has previously been observed in the homologous bacterial *Sa*CrtM.

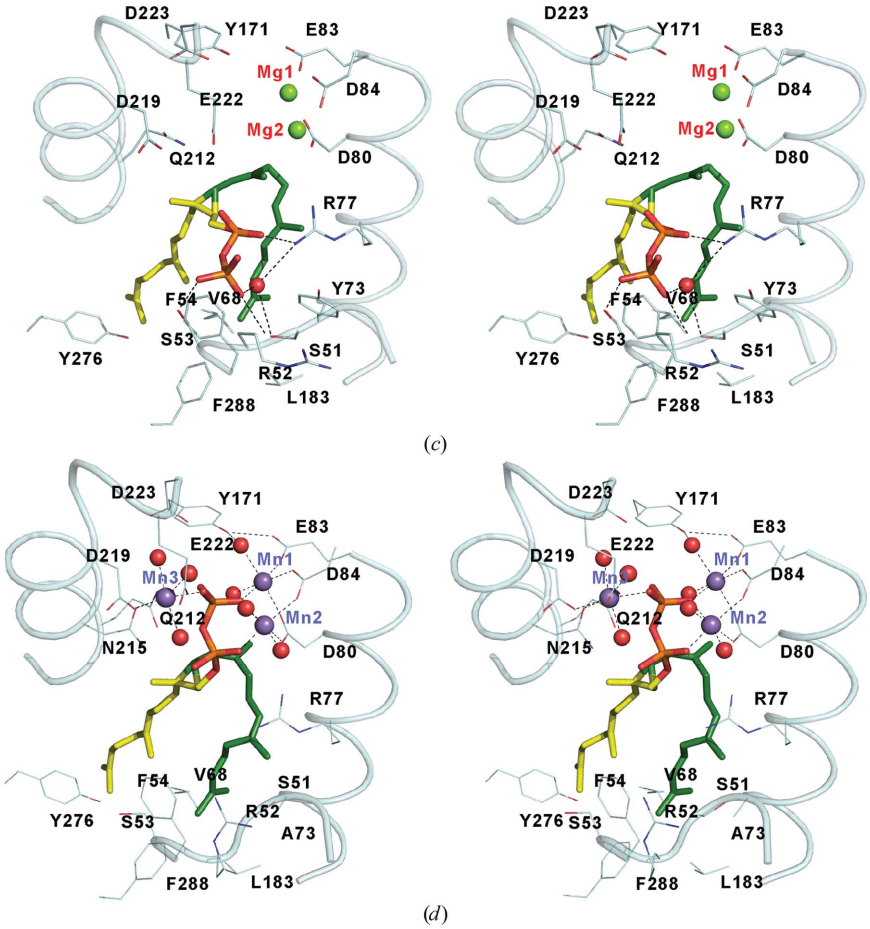

Figure 3 (continued)
(*b*) Stereoview of FsPP bound to *h*SQS in the presence of Mg^{2+} (PDB entry 3weg). (*c*) Stereoview of PSPP bound to *h*SQS in the presence of Mg^{2+} (PDB entry 3weh). (*d*) Stereoview of PSPP bound to *h*SQS (Y73A) in the presence of Mn^{2+} (PDB entry 3wei).

3.2.3. Step 3: opening the cyclopropane ring. The second half-reaction of SQSs can be triggered by the departure of the pyrophosphate group from PSPP. In *Sa*CrtM, Lin and coworkers proposed that PSPP switches to the 'activating binding site' for dissociation of the C1—O diphosphate bond and undergoes a rearrangement to yield the final product dehydrosqualene, which is also the major product that yeast, *Arabidopsis* and mouse SQS turn out in the absence of NADPH and in the presence of Mn^{2+} (Nakashima *et al.*, 1995; Jarstfer *et al.*, 2002; Busquets *et al.*, 2008). Mn^{2+}, which is an analogue of the biologically relevant Mg^{2+} ion, was shown to be six times more effective than Mg^{2+} in driving the formation of dehydrosqualene when NADPH was omitted in *y*SQS (Takatsuji *et al.*, 1982).

Several studies also showed that NADPH accelerated PSPP synthesis, although the reduced cofactor is not required for the first half-reaction (Zhang *et al.*, 1993; Mookhtiar *et al.*, 1994). However, we were unable to obtain the structure of the pyrophosphate group of PSPP bound near the Asp-rich motifs in the wild-type enzyme, even in the presence of Mg^{2+} with $NADP^{+}$ or its analogues. We assume that this ligand switch would be triggered elegantly by protein conformational change if NADPH is present. We then created the Y73A mutant, which has a broader S1 site to tolerate ligand movement, for cocrystallization with PSPP at an elevated level of Mn^{2+}. The 1.97 Å resolution structure provides a snapshot of the relocated PSPP in the activating site (Figs. 2*h* and 3*d*). Similar to the pyrophosphate group of the S1 FsPP bound in the activating site, the pyrophosphate moiety of the triterpene PSPP was chelated by two D*XX*ED motifs through a trio of Mn^{2+} bridges. $Mn1^{2+}$, $Mn2^{2+}$and $Mn3^{2+}$ reside at close positions to $Mg1^{2+}$, $Mg2^{2+}$ and $Mg3^{2+}$. Each metal site exhibits an octahedral coordination. The two farnesyl tails of PSPP remain in the S1 and S2 sites and its cyclopropane ring presents a slight shift of approximately 0.7 Å. Furthermore, the guanidinium group of Arg77, which formed a salt-bridge interaction with the α-phosphate O atom, might be involved in providing electrostatic assistance to the cleavage of the C—O bond in PSPP. With the departure of the pyrophosphate head group from PSPP, the cyclopropylcarbinyl cation is formed.

3.2.4. Step 4: critical amino acids for NADPH recognition. When the C1—O bond of PSPP is ruptured, the cyclopropylcarbinyl cation undergoes a rearrangement and is reduced by NADPH or NADH to yield squalene as the sole product (Supplementary Fig. S5). Studies of the control by NADPH of the regiochemistry and stereochemistry of the rearrangement of PSPP to 1′–1 squalene in *y*SQS have been extensively discussed (Blagg *et al.*, 2002; Pan *et al.*, 2009). How the NAD(P)H molecule reaches the active site remains unanswered and the structural basis of its binding pattern remains unclear. Attempts to obtain crystal structures of the enzyme–substrate–cofactor or enzyme–intermediate–cofactor complex were unsuccessful, possibly because of steric hindrance between FPP or PSPP and NADPH in the active site or because NADPH acts and leaves quickly during catalysis. *Sa*CrtM has no similar region to region IV of *h*SQS and performs NADPH-independent reactions. Based on structure and sequence comparisons with *Sa*CrtM, it has been proposed that the *h*SQS structure provides an additional cavity (the N site) for accommodating NADPH (Liu *et al.*, 2012). Judging by the electrostatic surface potentials, this proposed NADPH site is surrounded by many positively charged residues, including Arg52, Arg77, Arg218, Lys315, Arg317 and Lys318, which are probably involved in attracting if not directly interacting with the negatively charged parts of NADPH. Specific mutants were designed to determine the necessity of key amino-acid residues involved in the recognition of reduced nicotinamide cofactor (Supplementary Table S2). Mutational studies of the conserved Arg and Lys residues surrounding the cavity showed diverse effects on the reducing step. A dominant inhibitory effect of the R218A mutant on the reducing step was overcome using a high level of NADPH (Fig. 4*b*). It was established that the JK loop is particularly vital for the second half-reaction of SQS. The synergistic effects that were observed in the K315E/R317E and K315E/K318E mutants completely aborted squalene formation. Except for R52E, the defect in the reducing step can be rescued by using an excess amount of reduced NADPH. The substitution of Arg52 (on the AB flap) by Ala or Glu does not interfere with FPP consumption. However, the formation of squalene indicates that the guanidinyl moieties participate in NADPH recognition (Supplementary Table S2). Consequently, the structural and biochemical results obtained in this study demonstrate that there is ample space and that there are ample interactions,

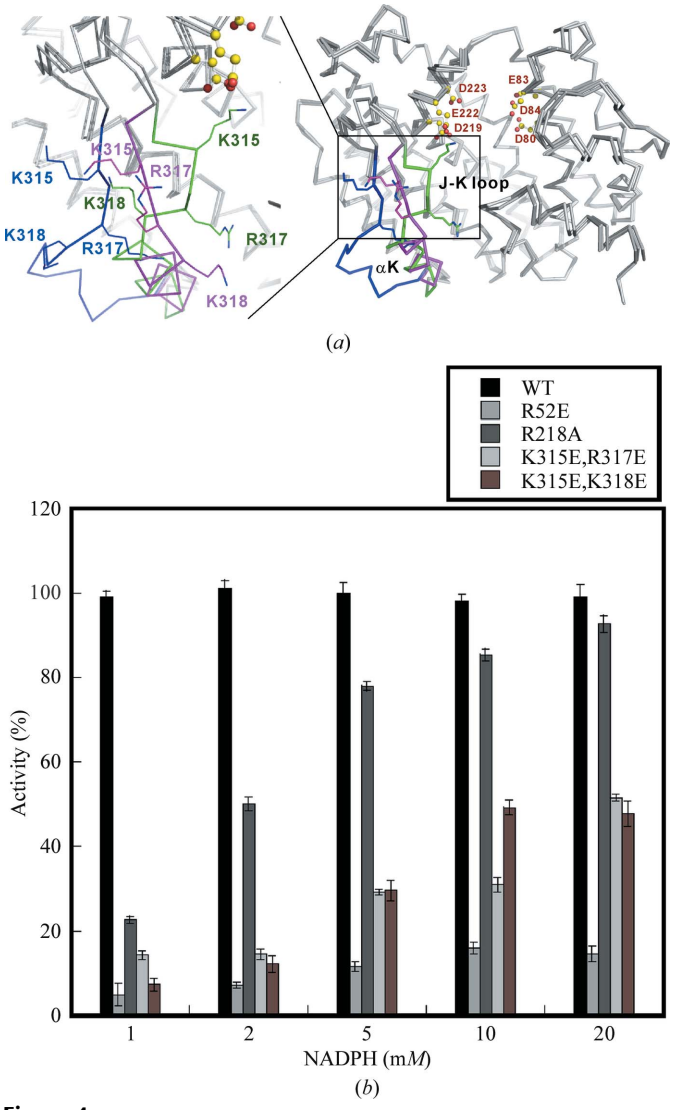

Figure 4
(*a*) Three different conformations of the JK loop in *h*SQS. The structures of mode 1 (magenta) belong to space group $P2_12_12_1$, mode 2 (which presents a 'loop-in' or 'locally closed' form; green) belongs to space group $P2_12_12$ and mode 3 (which might be caused by crystal packing; blue) belongs to space group $P2_1$. In mode 2, the side chains of Lys315 and Arg317 are oriented towards the active site. Two aspartate-rich motifs are shown as ball-and-stick models. (*b*) Percentage of rescued activity in the *h*SQS mutants using an increased NADPH dosage.

particularly in region IV, to accommodate NADPH in the active site.

3.3. Characterization of the Phe288 mutants

In previous reports, the replacement of Phe288 by other charged or small residues resulted in a pronounced elimination of SQS activity in rat and plants (Gu *et al.*, 1998; Akamine *et al.*, 2003; Busquets *et al.*, 2008). In *h*SQS, the end of the central cavity is surrounded by large amino acids such as Val69, Leu183, Phe187, Tyr276 and Phe288. Consistent with previous studies, the substitution of Phe288 by Ala significantly reduced the enzyme activity (Supplementary Table S2). To assess the contribution of Phe288 to control of the conversion of FPP to PSPP and squalene production, we designed further mutants and determined their crystal structures in complexes with PSPP to investigate its catalytic role.

The crystal structure of the F288A mutant in complex with PSPP was determined at 2.0 Å resolution and was refined to a crystallographic *R* factor of 20.8%. The Ala substitution is clearly visible in the electron-density map, as is the binding conformation of PSPP (Fig. 5*a*). The replacement of Phe288 by a small residue results in a deeper cleft, indicating that Phe288 acts as a floor for the S1 site. If the aromatic ring is omitted, the S1 hydrocarbon group of the PSPP in the F288A mutant moves downwards by approximately 4.5 Å, resulting in a mis-orientation of the α-phosphate group from Arg77 (Figs. 5*a* and 5*b*). However, the F288L mutant retained much of the first-step enzyme activity and approximately 50% of the second-step activity. Except for the diphosphate headgroup, the conformation of PSPP is nearly identical to that observed in wild-type *h*SQS (Figs. 5*c* and 5*d*). This finding implicates Phe288 not only in assisting in substrate ionization but also in stabilizing PSPP by subtle electrostatic and structural properties in the second half-reaction. Unexpectedly, the

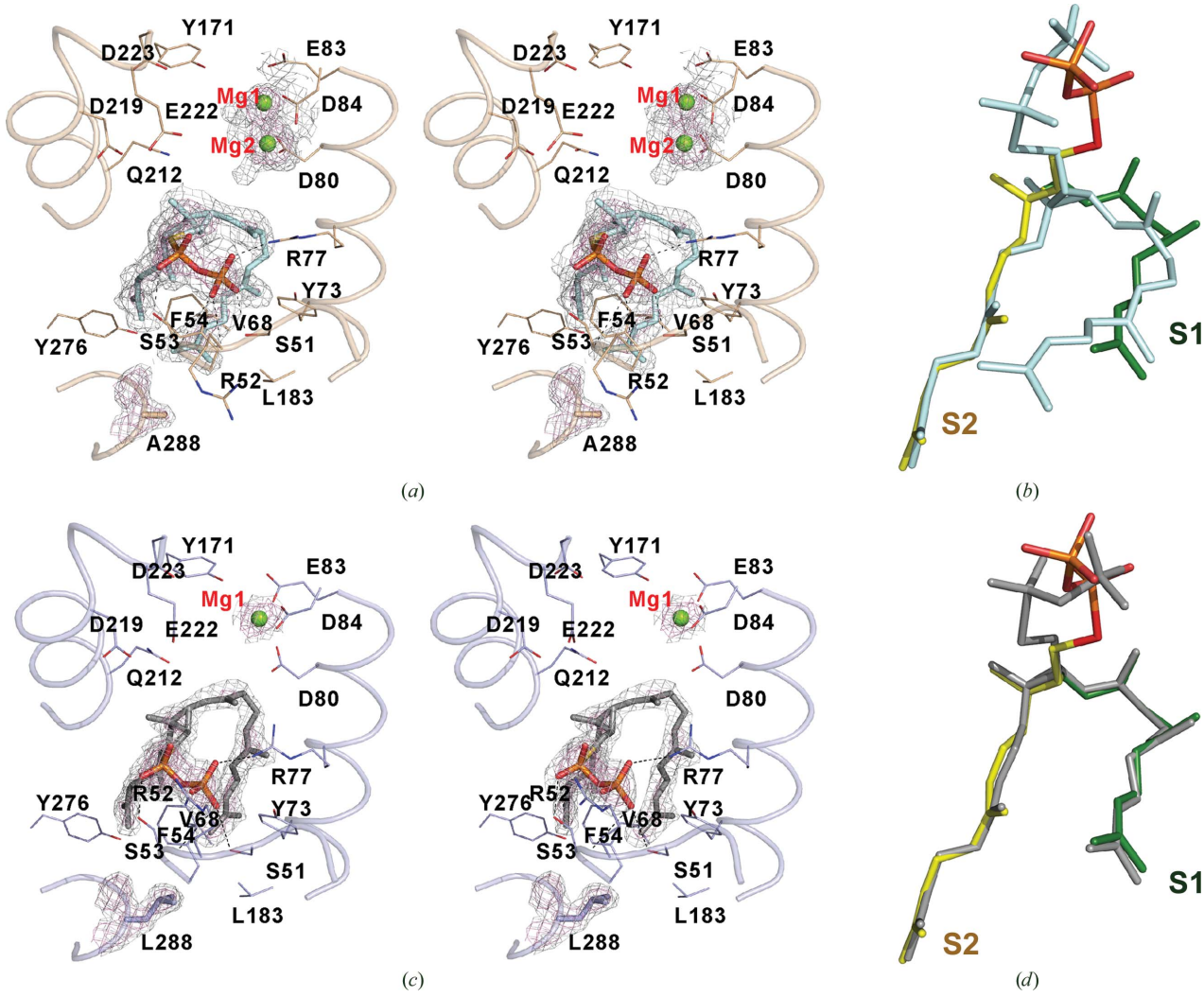

Figure 5
Variation of intermediate binding modes of the *h*SQS mutants. (*a*) The final $2F_o - F_c$ electron-density maps for PSPP (cyan) and residue Ala288 at 2.0 Å resolution are contoured at 1.0σ (grey) and 2.0σ (pink). (*b*) Comparison of binding modes of PSPP between the F288A mutant and wild-type *h*SQS (green and yellow). (*c*) PSPP binding in the active site of the F288L mutant. The final $2F_o - F_c$ electron-density maps for PSPP (grey) and residue Leu288 at 1.85 Å resolution are contoured at 1.0σ (grey) and 2.0σ (pink). (*d*) Superimposition of the F288L mutant and wild-type *h*SQS (green with yellow) illustrates the similar binding conformation of PSPP.

*h*SQS-(F288L)–PSPP–Mg^{2+} structure exhibits a well ordered JK loop-in conformation, migrating nearly 5 Å towards the active site. For *h*SQS, three major conformations of the JK loop were observed, as shown in Fig. 4(*a*). We assume that the flexibility of the JK loop and helix αK may contribute to the recruitment of NAD(P)H to reach the active site in the second half-reaction.

4. Proposed NADPH binding mode

After PSPP releases its pyrophosphate moiety to form the C1′–C2–C3 cyclopropylcarbinyl cation, subsequent reactions incorporate a hydride from NADPH to yield squalene. Region IV of the SQS enzyme presents no homology to known pyridine dinucleotide-binding motifs, indicating that SQS might adopt a distinct NADPH binding mode from the Rossmann fold in the active site. Poulter and coworkers proposed that SQS contains one or two overlapping catalytic sites to perform both half-reactions. PSPP formation was accelerated by NADPH and excess FPP (a third unreactive FPP) by binding to the same region (Radisky & Poulter, 2000). At the beginning of the second half-reaction, PSPP remains in the activating binding site, indicating that the 'non-activating binding site' is empty. Further, a reduced nicotinamide cofactor must be close to the cyclopropane ring to donate a hydride and to reduce PSPP. Based on the *h*SQS-(Y73A)–PSPP–Mn^{2+} (PSPP in the activating site) and *h*SQS-(F288L)–PSPP–Mg^{2+} (JK loop-in conformation) structures, the proposed binding cavity might be constituted by regions I and IV, creating a multiply positively charged environment for stabilizing the negatively charged phosphate groups in NADPH, including Lys315 and Arg317, which are in the JK loop. The site-directed mutagenesis results support Arg52, Arg218, Lys315 and Lys318 acting as primary residues in the second half-reaction. The synergistic inhibition effect observed in the K315E/R317E and K315E/K318E double mutants resulted in complete elimination of enzyme activity (Supplementary Table S2). Moreover, a high level of NADPH failed to overcome the double-mutant defect in the reducing step, particularly in R52E (Fig. 4*b*). Combining the mutagenesis and structural data, we therefore propose a model for NADPH bound in the active site in which NADPH is likely to orient itself in such a way that the nicotinamide is now located near the cyclopropane ring (Figs. 6*a*–6*c*). After the C—O diphosphate bond in bound PSPP is ruptured, the negatively charged pyrophosphate ion might move close to the conserved Asn215 and Arg218, while the reduced nicotinamide transfers a hydride ion to the C1′ position of the cationic intermediate to form the respective 1′–1 product squalene.

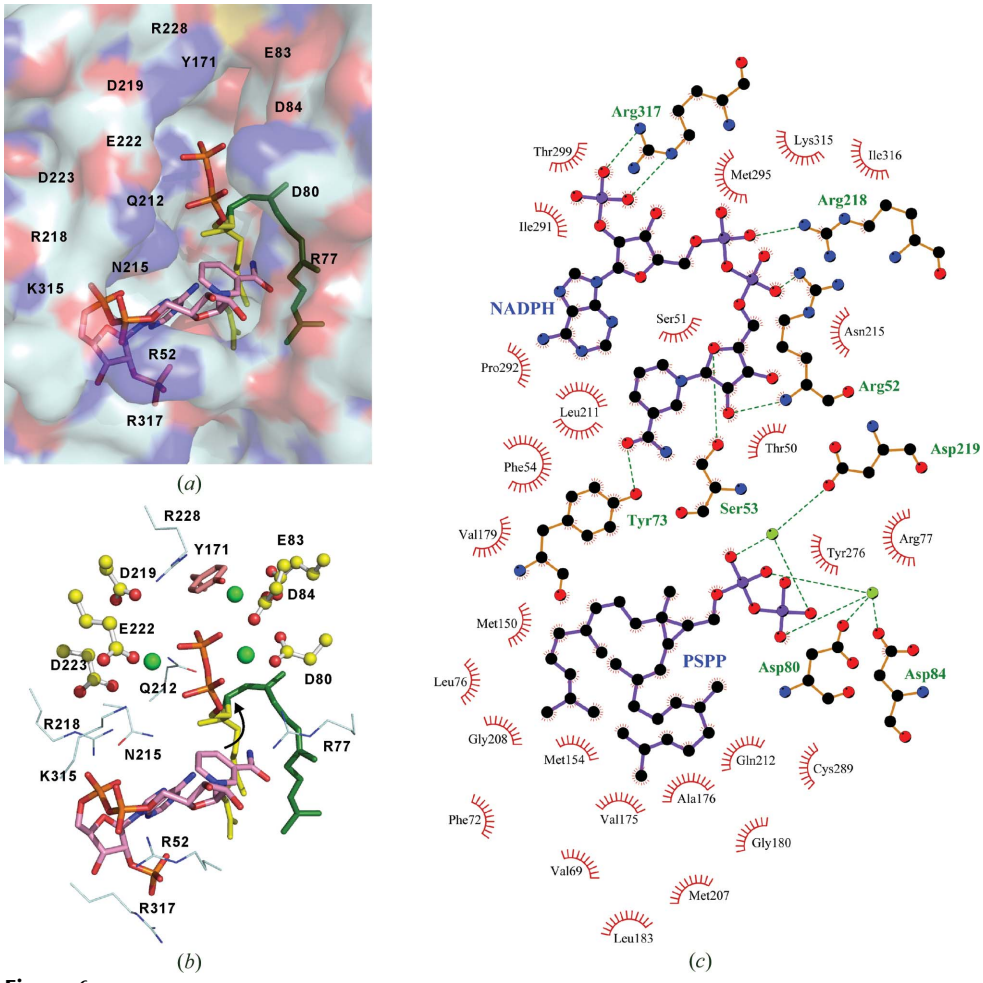

Figure 6
Putative NADPH binding mode. (*a*) Electrostatic surface-potential representation of the active site. PSPP is shown in yellow and green. NADPH is shown in pink. The nicotinamide ring is close to the cyclopropane ring. Mg^{2+} ions are presented as green balls. (*b*) Residues lining the active-site pockets are shown as thin sticks. The two Asp-rich motifs are shown in ball-and-stick representation. In this model, NADPH can transfer hydride to the cyclopropane C atom (arrow). (*c*) Residues in *h*SQS that interact with PSPP and NADPH as predicted by *LIGPLOT* (Wallace *et al.*, 1995). Hydrogen-bonding interactions are shown as green dashed lines. Green spheres represent Mg^{2+} ions. Residues involved in hydrophobic contacts are denoted by curved combs.

5. Conclusion

The structural snapshots of the SQS reaction steps observed in this study support the mechanism proposed for *Sa*CrtM, indicating that the process is a common feature of the biogenesis of isoprenoids with a 1′–1 linkage. Our model for the reaction of 'head-to-head' terpene synthases is depicted in Supplementary Fig. S6. At the beginning of the reaction, an alkyl substrate (*e.g.* the

C_{15} FPP or the C_{20} GGPP) is bound in the 'non-activating binding site' (S2 site) and creates an 'activating site' (S1 site) for accommodation of the allylic substrate. As the allylic substrate becomes activated by a trio of Mg^{2+} ions, the formed allylic cation moves towards the alkyl acceptor. In the condensation step, the allylic cation is added to the alkyl substrate by an electrophilic attack on the C2═C3 double bond, resulting in a cyclopropylcarbinyl diphosphate with a C1′–C2–C3 structure. In this manner, the C_{15} FPP yields the C_{30} prehydrosqualene diphosphate (PSPP) and the C_{20} GGPP yields the C_{40} prephytoene diphosphate (PPPP). In the second reaction, the pyrophosphate of PSPP and PPPP switches from the 'non-activating' to the 'activating' binding site and is ionized again. After the rearrangement, PSPP forms dehydrosqualene in *Sa*CrtM or is further reduced to produce squalene in SQS, and PPPP is converted to phytoene. Finally, we assume that similar reactions might also be adopted by botryococcene synthase from green microalga in synthesizing the C_{30} botryococcene from the C_{15} FPP, also *via* a PSPP intermediate (Okada *et al.*, 2004).

We thank the National Synchrotron Radiation Research Center in Taiwan and SPring-8 and Photon Factory in Japan for beam-time allocations and data-collection assistance. This work was supported by Academia Sinica and the National Science Council, Taiwan (grants NSC96-3114-P-001-004, NSC97-3114-P-0010-001 and NSC99-3113-B-001-001 to AH-JW).

References

Akamine, S., Nakamori, K., Chechetka, S. A., Banba, M., Umehara, Y., Kouchi, H., Izui, K. & Hata, S. (2003). *Biochim. Biophys. Acta*, **1626**, 97–101.

Blagg, B. S., Jarstfer, M. B., Rogers, D. H. & Poulter, C. D. (2002). *J. Am. Chem. Soc.* **124**, 8846–8853.

Busquets, A., Keim, V., Closa, M., del Arco, A., Boronat, A., Arró, M. & Ferrer, A. (2008). *Plant Mol. Biol.* **67**, 25–36.

Cao, R., Zhang, Y., Mann, F. M., Huang, C., Mukkamala, D., Hudock, M. P., Mead, M. E., Prisic, S., Wang, K., Lin, F.-Y., Chang, T.-K., Peters, R. J. & Oldfield, E. (2010). *Proteins*, **78**, 2417–2432.

Dogbo, O., Laferriére, A., D'Harlingue, A. & Camara, B. (1988). *Proc. Natl Acad. Sci. USA*, **85**, 7054–7058.

Emsley, P. & Cowtan, K. (2004). *Acta Cryst.* D**60**, 2126–2132.

Gu, P., Ishii, Y., Spencer, T. A. & Shechter, I. (1998). *J. Biol. Chem.* **273**, 12515–12525.

Guo, R.-T., Cao, R., Liang, P. H., Ko, T.-P., Chang, T.-H., Hudock, M. P., Jeng, W.-Y., Chen, C. K.-M., Zhang, Y., Song, Y., Kuo, C.-J., Yin, F., Oldfield, E. & Wang, A. H.-J. (2007). *Proc. Natl Acad. Sci. USA*, **104**, 10022–10027.

Hyatt, D. C., Youn, B., Zhao, Y., Santhamma, B., Coates, R. M., Croteau, R. B. & Kang, C. (2007). *Proc. Natl Acad. Sci. USA*, **104**, 5360–5365.

Iwata-Reuyl, D., Math, S. K., Desai, S. B. & Poulter, C. D. (2003). *Biochemistry*, **42**, 3359–3365.

Jarstfer, M. B., Zhang, D.-L. & Poulter, C. D. (2002). *J. Am. Chem. Soc.* **124**, 8834–8845.

Kahlon, A. K., Roy, S. & Sharma, A. (2010). *J. Biomol. Struct. Dyn.* **28**, 201–210.

Lee, S. & Poulter, C. D. (2008). *J. Bacteriol.* **190**, 3808–3816.

Liang, P.-H. (2009). *Biochemistry*, **48**, 6562–6570.

Lin, F.-Y., Liu, C.-I., Liu, Y.-L., Zhang, Y., Wang, K., Jeng, W.-Y., Ko, T.-P., Cao, R., Wang, A. H.-J. & Oldfield, E. (2010). *Proc. Natl Acad. Sci. USA*, **107**, 21337–21342.

Lin, F.-Y., Zhang, Y., Hensler, M., Liu, Y.-L., Chow, O. A., Zhu, W., Wang, K., Pang, R., Thienphrapa, W., Nizet, V. & Oldfield, E. (2012). *ChemMedChem*, **7**, 561–564.

Liu, C.-I., Jeng, W.-Y., Chang, W.-J., Ko, T.-P. & Wang, A. H.-J. (2012). *J. Biol. Chem.* **287**, 18750–18757.

Lovell, S. C., Davis, I. W., Arendall, W. B. III, de Bakker, P. I., Word, J. M., Prisant, M. G., Richardson, J. S. & Richardson, D. C. (2003). *Proteins*, **50**, 437–450.

Mookhtiar, K. A., Kalinowski, S. S., Zhang, D. & Poulter, C. D. (1994). *J. Biol. Chem.* **15**, 11201–11207.

Murshudov, G. N., Skubák, P., Lebedev, A. A., Pannu, N. S., Steiner, R. A., Nicholls, R. A., Winn, M. D., Long, F. & Vagin, A. A. (2011). *Acta Cryst.* D**67**, 355–367.

Nakashima, T., Inoue, T., Oka, A., Nishino, T., Osumi, T. & Hata, S. (1995). *Proc. Natl Acad. Sci. USA*, **92**, 2328–2332.

Okada, S., Devarenne, T. P., Murakami, M., Abe, H. & Chappell, J. (2004). *Arch. Biochem. Biophys.* **422**, 110–118.

Otwinowski, Z. & Minor, W. (1997). *Methods Enzymol.* **276**, 307–326.

Pan, J.-J., Bugni, T. S. & Poulter, C. D. (2009). *J. Org. Chem.* **74**, 7562–7565.

Pandit, J., Danley, D. E., Schulte, G. K., Mazzalupo, S., Pauly, T. A., Hayward, C. M., Hamanaka, E. S., Thompson, J. F. & Harwood, H. J. Jr (2000). *J. Biol. Chem.* **275**, 30610–30617.

Pelz, A., Wieland, K. P., Putzbach, K., Hentschel, P., Albert, K. & Götz, F. (2005). *J. Biol. Chem.* **280**, 32493–32498.

Perzl, M., Reipen, I. G., Schmitz, S., Poralla, K., Sahm, H., Sprenger, G. A. & Kannenberg, E. L. (1998). *Biochim. Biophys. Acta*, **1393**, 108–118.

Radisky, E. S. & Poulter, C. D. (2000). *Biochemistry*, **39**, 1748–1760.

Rilling, H. C. (1966). *J. Biol. Chem.* **10**, 241, 3233–3236.

Rondeau, J. M., Bitsch, F., Bourgier, E., Geiser, M., Hemmig, R., Kroemer, M., Lehmann, S., Ramage, P., Rieffel, S., Strauss, A., Green, J. R. & Jahnke, W. (2006). *ChemMedChem*, **1**, 267–273.

Starks, C. M., Back, K., Chappell, J. & Noel, J. P. (1997). *Science*, **277**, 1815–1820.

Takatsuji, H., Nishino, T., Izui, K. & Katsuki, H. (1982). *J. Biochem.* **91**, 911–921.

Vagin, A. & Teplyakov, A. (2010). *Acta Cryst.* D**66**, 22–25.

Vaguine, A. A., Richelle, J. & Wodak, S. J. (1999). *Acta Cryst.* D**55**, 191–205.

Wallace, A. C., Laskowski, R. A. & Thornton, J. M. (1995). *Protein Eng.* **8**, 127–134.

Winn, M. D. *et al.* (2011). *Acta Cryst.* D**67**, 235–242.

Zhang, D., Jennings, S. M., Robinson, G. W. & Poulter, C. D. (1993). *Arch. Biochem. Biophys.* **304**, 133–143.

Zhao, R.-Y., Xiao, W., Cheng, H.-L., Zhu, P. & Cheng, K.-D. (2010). *J. Ind. Microbiol. Biotechnol.* **37**, 1171–1182.